Saudi Journal of Biological Sciences 29 (2022) 460–471

Contents lists available at ScienceDirect

Saudi Journal of Biological Sciences

journal homepage: www.sciencedirect.com

Original article

Green synthesis of silver nanoparticles by *Conocarpus Lancifolius* plant extract and their antimicrobial and anticancer activities

Mohammad Oves [a,1,*], Mohd Ahmar Rauf [b,1], Mohammad Aslam [a], Huda A Qari [a,c], Hana Sonbol [d], Irfan Ahmad [e], Gaffar Sarwar Zaman [e], Mohd Saeed [f,*]

[a] Center of Excellence in Environmental Studies, King Abdul Aziz University, 21589 Jeddah, Saudi Arabia
[b] Use-Inspired Biomaterials & Integrated Nano Delivery (U-Bind) Systems Laboratory, Department of Pharmaceutical Sciences, Eugene Applebaum College of Pharmacy and Health Sciences, Wayne State University, Detroit, MI 48201, USA
[c] Department of Biological Science, Faculty of Science, King Abdul-Aziz University, 21589 Jeddah, Saudi Arabia
[d] Biology Department, Faculty of Science, Princess Nourah bint Abdulrahman University, Riyadh, Saudi Arabia
[e] Department of Clinical Laboratory Sciences, College of Applied Medical Sciences, King Khalid University, Abha, Saudi Arabia
[f] Department of Biology, College of Sciences, University of Hail, Hail, Saudi Arabia

ARTICLE INFO

Article history:
Received 14 July 2021
Revised 2 September 2021
Accepted 5 September 2021
Available online 13 September 2021

Keywords:
Conocarpus Lancifolius
Green synthesis
Silver nanoparticles
Antibacterial
Antifungal
Anticancer agent

ABSTRACT

Due to drug addiction and the emergence of antibiotic resistance in pathogens, the disease load and medication intake have risen worldwide. The alternative treatment for drug-resistant infections is Nano formulation-based antimicrobial agents. The plant extract of Conocarpus Lancifolius fruits was used to synthesize silver nanoparticles in the current study, and it was further employed as an antimicrobial and anticancer agent. Nanoparticles have been characterized by UV–visible spectrometer revealed the notable peak of λ_{max} = 410–442 nm, which confirms the reduction of silver ion to elemental silver nanoparticles, and the biological moieties in the synthesis were further confirmed by FTIR analysis. The stability and crystalline nature of materials were approved by XRD analysis and expected the size of the nanomaterials of 21 to 173 nm analyzed by a nanophox particle-size analyzer. In vitro, synthesized materials act as an antibacterial agent against *Streptococcus pneumonia* and *Staphylococcus aureus.* The inhibition zones of 18 and 24 mm have been estimated to be antibacterial activity against both bacteria. The potency of up to 100% of AgNPs for bacterial strains was incubated overnight at 60 µg/ml. Based on our results, biogenic AgNPs reveal significant activity against fungal pathogen *Rhizopusus stolonifera* and *Aspergillus flavus* that cause leading infectious diseases. Additionally, nanomaterials were biocompatible and demonstrated the potential anticancer activities against MDA MB-231 cells after 24-hour exposure.

1. Introduction

The study and application of nanomaterials are increasing day by day in recent years since the Nano-size object shows differing properties of its bulk materials because of changes in its surface-volume ratio (Yaqoob et al., 2020). In many biochemical reactions and numbers of applications in different industries, most nanomaterials have shown excellent quantum confinement with unique catalysis properties to improve the technique for electronic, environmental, and biomedical purposes(Maduraiveeran et al., 2018). Biologically nanomaterials are used in bio-imaging, diagnosis, bio-sensing, gene therapy, antimicrobial and anticancer medications (Oves et al., 2019).

Greener nanoparticle synthesis represents a step forward over other methods because it is straightforward, cost-effective, and relatively reproducible, and frequently results in more stable materials. Microorganisms can also be used to synthesize nanoparticles. Still, the synthesis rate is slower, and the method is limited in terms of available sizes and shapes compared to routes involving plant-based materials. There is no requirement for high pressure, energy, temperature, or toxic chemicals in the green synthesis method. As a result, many researchers are now abandoning syn-

* Corresponding authors.
E-mail addresses: owais.micro@gmail.com (M. Oves), mmateenuddin@kau.edu.sa, mo.saeed@uoh.edu.sa (M. Saeed).
[1] Equal contribution from the authors.
Peer review under responsibility of King Saud University.

Production and hosting by Elsevier

https://doi.org/10.1016/j.sjbs.2021.09.007
1319-562X/

thetic methods. Plants produce more stable nanoparticles than other methods and are very easy to scale up.

Additionally, the risk of contamination is reduced (Barakat et al., 2020; Swilam and Nematallah, 2020; Bindhu et al., 2020; Rohaizad et al., 2020; Renuka et al., 2020; Qayyum et al., 2017). It is necessary to preserve the bio-compatibility of synthesized nanomaterials because chemically synthesized materials have multiple human health and environmental drawbacks (Swilam and Nematallah, 2020; Bindhu et al., 2020; Rohaizad et al., 2020; Renuka et al., 2020; Qayyum et al., 2017).

Silver nanoparticles (AgNPs) are intriguing nanomaterials that show particular promise in fields such as colourimetric sensors, bactericidal materials, and electrochemical sensor components. Unlike gold nanoparticles, silver nanoparticles can be easily synthesized from relatively stable silver (I) salts using various reducing agents. The antimicrobial efficacy of nano silver-based biomaterials was evaluated experimentally against a wide range of medically significant planktonic and sessile-pathogenic microorganisms, including bacteria, viruses, fungi and yeasts. The remarkable antimicrobial activity of AgNPs provides a strong foundation for the design, manufacture and implementation of novel and performance-enhancing nano silver-based biomedical products, such as anticancer agents, drug delivery systems, orthopaedic materials and devices, bandages, antiseptic sprays and catheters. As a result of the remarkable versatility of AgNPs in nanotechnology, biomedicine and the environment, there is a constant need to develop cost-effective AgNP synthesis methods. The translation of silver-based nanotechnology into clinical applications requires not only the development of safe, simple, environmentally friendly and cost-effective methods for the synthesis of silver nanoparticles but also a deep understanding of the associated physicochemical peculiarities, in vitro and in vivo effects, biodistribution, safety controls, pharmacokinetics and pharmacodynamics.

Conocarpus Lancifolius plant fruit was selected for the active molecule extraction and green synthesis of silver nanomaterials and application as an antimicrobial anticancer agent in this study.

The plant *Conocarpus Lancifolius* belonged to the genus *Conocarpus* and the family Combretaceae (“Genus: Conocarpus L.”, , 1996–09-17.; Duke, 1996). *C. Lancifolius* species is restricted only to the southern Red sea Coasts, and other species of the same genus are *Conocarpus erectus.* It is widespread in tropical America, Bermuda, Southern Florida, Bahamas, South Mexico, Peru, Congo. The *C. Lancifolius* plants were primarily native to Djibouti’s coastal and riverine areas, Somalia, Yemen. It is also found in the Horn of Africa, South Asia, and the Arabian peninsula (Conocarpus lancifolius - Geographic range in detail“. IUCN Red List., 1998). *C. Lancifolius* plant has multiple trunks and grows like shrubs and is planet-sized from 1 to 20 m tall. The name also knows *C. Lancifolius* of ”Damas“ in Arabic and ”Qalab“ in Somali. It’s commonly used in the garden in residential compounds and street roadside plants in the gulf region. These plants are a pioneering species in reforestation because it has high salinity tolerance and drought tolerance. The tree thrives exceptionally well in the hot and dry climate of the city. Its young leaves contain high tannin, sometimes used for fodder for animals.

In this study, we choose *C. Lancifolius* because it has potential medicinal value in the native countries of this plant. Its leaf extract is used in anaemia, conjugative inflammatory, catarrh, diarrhoea, diabetes, fever, bleeding, skin ulcers, and syphilis orchitis treatment (Al-Taweel et al., 2016). In a study, these plant extracts can decrease glucose levels in rabbits’ blood if they have previously induced diabetes (Khan and Khan, 2017). Besides, *C. Lancifolius* fruits extract has excellent cytotoxicity against cancer cell line MRC-5 (Mohammed et al., 2019). In previous studies, the leave, fruit, bark, stem extract of *C. erectus* was used for Gram-Positive and Gram-negative bacteria (Ali et al., 2013). Conocarpus Lancifolius Aqueous leaves extract has recently been used for hemolytic Cytotoxicity and Antibacterial Activity against pathogenic bacteria and antiplasmodial; antileishmanial antitrypanosomal activities (Mohammed et al., 2019). Chemical analysis of plant extract has contained nine alkaloid compounds and five saponins compounds, and eight compounds belong to the phenolic compounds by chromatography (Othman et al., 2019).

Conocarpus Lancifolius fruits have been collected from the mature plant and used for active molecule extraction and green synthesis of silver nanomaterials in this study. For our study we obtained the plant leaves and fruits from the botanical garden of our university. The green synthesized nanomaterials have been characterized for structural and morphological characterization and used as an antimicrobial and anticancer agent.

2. Materials methods

2.1. Chemicals and reagents

In this investigation, most of the chemicals are analytical grade; Silver nitrate was obtained from La Pine Science Corporation (Chicago, America). Nutrient broth and culture media were obtained from the HI Media (Pvt. Ltd. Mumbai. India). Bacterial and fungal microorganisms were procured from the culture library of the laboratory and King Abdul-Aziz University.

2.2. Conocarpus Lancifolius fruits collection and extracts preparation

From the mature plant of the roadside plantation of King Abdul-Aziz University Campus Jeddah, KSA, the *Conocarpus Lancifolius* fruits were collected. The plant leaves were removed from the stem and washed with Milli-Q water three times and in an aqueous solution one time with 75 percent ethanol. These clean leaves were dried at 60 °C in a vacuum oven (JSOF-100H, JS Research Inc. Korea) and milled into a FOSS cyclotec 1093 sample mill (80 mm mesh size) and obtained a fine powder. This fine powder, up to 5 g was transferred into a 500 ml beaker contains 250 ml of deionized water and boiled at 110 °C for 20 min. The beaker solutions were cooled at room temperature, purified under vacuum through grade 1 filter paper and further filtered through a 0.25 mm syringe filter to eliminate particulate materials and deposited at 4 °C for potential use depicted in Fig. 1.

2.3. Silver nanoparticles synthesis by the bottom-up approach.

In this study, silver nanoparticles were synthesized by the green synthesis route of the bottom-up approach and methodology slightly different from the previous studies (Oves et al., 2018; Qayyum et al., 2017). Briefly, 250 ml of 0.1 mM aqueous silver nitrate solution containing bottle was cooled 2 h at 0 °C in the refrigerator. Separately, 250 ml of plant leaves extract containing beaker was placed on the magnetic stirring and drop-wise addition of cooled silver nitrate solution and monitor the reduction of Ag + ions into Ag^0 at room temperature of 30 ^{0}C. The solution colour changed from light yellow to dark yellow and looking colloidal brown after the overnight incubation, and a UV–visible spectrometer was used to monitor these colour changes (UV-1800, Shimadzu, Japan). To avoid the precipitation of $AgNO_3$, most of the solutions were made in ultra-pure chlorine-free water, and the reaction set was also equipped in the dark to prevent photoactivation. This reaction mixture was centrifuged three times at 10,000 rpm for 30 min. after centrifuge, the obtained pellets were collected and dried in a vacuum oven at 80 ^{0}C. This powder was sealed, packed in glass vials, and appropriately stored at 4 °C for characterization.

Fig. 1. Depiction of plant *Conocarpus Lancifolius* with (i) fruits bunch, (ii) dried fruits, (iii) fruits powder (iv) aqueous fruit extract in a bottle.

2.4. Characterization of AgNPs

2.4.1. UV–visible spectroscopy.

The silver ion reduction from the plant's extract as a substrate mixture and a prepared colloidal mixture of AgNPs was optimized by the UV–vis absorption spectra as a time and temperature function. Around 10 ml of the brown reaction mixture has routinely been used to track the bioreduction of Ag + in an aqueous solution for examination. Tests were made for UV–vis spectrums at variable temperature range of 10 to60 °C and 5 – 90 min incubation time.

2.4.2. X-ray diffraction (XRD)

Crystal study of fine AgNPs was conducted via X-ray diffraction patterns. XRD was performed with Cu-Kα radiation (l = 0.15406 n m) using an X-pert X-ray powder diffractometer (Philips PW1398) in the 2 θ range 20 to 80°.

2.4.3. Ftir spectroscopy

Fourier transforms Infra-red (IRAffinity-1, Shimadzu, Japan) spectra for synthesized nanomaterials have also been studied by Fourier transforms. Samples of AgNPs were prepared with the KBr crystal as a beam splitter to determine the position of biological entities involved in particle synthesis. The sample was centrifuged for 10 min at 10,000 rpm, and the resulting pellets were dried at 80° C and grounded to remove undesirable plant materials and silver with KBr crystal. The spectra of AgNPs were recorded as a KBr pellet at a resolution of 4 cm^{-1} in the wavenumber region of 400–4000 cm^{-1}.

2.4.4. Electron microscopy and energy dispersive X-ray

The biogenic nanomaterials were characterized using Scanning Electron Microscopy (SEM, JSM-7900F, JEOL Ltd, Japan). Samples of the AgNPs were mounted on the grid using carbon or copper tape and sputtered with gold using a sputter coater (Quorum Q150R ES, Quorum Technologies Ltd. Ashford. Kent. England). The voltage was set at 15 kV and magnification 10000X. The attached sample's basic information was observed by dispersive energy X-ray (EDAX) (Amtech GmbH, Wiesbaden, Germany). Besides this, transmission electron microscopy also confirmed the nanoparticles' size and shape (TEM, JEOL JEM-1011, Japan).

3. Antimicrobial activity

3.1. Zone inhibition assay

The antimicrobial properties of biogenic nanomaterial were tested against bacteria and fungi. In this study, *Streptococcus pneumonia* and *Staphylococcus aureus* were used for antibacterial testing. In contrast, *Rhizopusus stolonifera* and *Aspergillus flavus* were used for antifungal testing. In 2% peptone broth and 1.4% nutrient broth, respectively, the fungi and bacterial strains were inoculated and put overnight at 35 °C in an incubator to achieve a new culture. Development inhibition experiments were conducted using Bauer's diffusion method in both liquid and solid agar plate medium. The medium used is sterile, and bacteria were incubated and transferred according to McFarland's vial culture procedure. The McFarland Protocol is used as a primary reference to assess bacterial concentration in the samples. To maximize these microorganisms' growth, bacteria and fungi were distributed on nutrient agar and Czapk media, respectively. The plates used a high content culture, and the 6 mm bore samples were later capped with agar solution. AgNPs were put in the wells and incubated overnight at 37 °C; 50 µl of the medium was applied to each well. Fluconazole was used as the positive control against bacteria.

3.2. Fungal growth assay

The Biogenic synthesized silver nanomaterial was centrifuged and oven-dried, and 100 mg stock solution was made in sterile water. AgNPs was amended in the Petri dish during the media's pour plate method from these stock solutions. Each plate's final concentration makes up 12.5, 25, 50, and 100 AgNPs μg/ml separately. The control contained only sterile water without AgNPs in the media. A fungus strain was inoculated in each PDA plate's centre, Petri plates were placed in the incubator for incubating at 37 °C for five days.

3.3. AgNPs potency against the bacterial strain

The effect of AgNPs on the growth of bacteria has been studied. At the end of each hour, a drop of culture was passed into a test tube for further testing. A comprehensive sequence of serial dilutions of 0.1 ml was prepared up to 5 times with sterile saline water on sterile nutrients agar plates. Three culture plates were primed and incubated overnight at 37° C. The bacterial colonies were counted the next day by colony counter (Colony Count V, Gerber Instruments AG, Effretikon, Switzerland).

3.4. AgNPs effect on the cell surface

The scanning electron microscope (FEI, Quanta FEG 450) revealed *Streptococcus pneumonia* and *Staphylococcus aureus* cell morphology. Samples of 1 ml colonies treated with AgNPs were harvested for this purpose and taken at Eppendorf and centrifuged for 10 min at 10000 rpm to detect pellet-shaped cells. The cells containing pellets have been cleaned three times with a phosphate saline buffer. Furthermore, washed cells were fixed overnight at 4° C in a 3% glutaraldehyde solution. Furthermore, 100 µl of the sample aliquots are washed three times with sterilized filtered water and centrifuged at 8000 rpm before mixed with 100 ml of cell pellet Milli Q water and spread on a glass slide. After glass slides were set and analyzed in FESEM, the sputter coater (Quorum Q150R ES, Quorum Technologies Ltd. Ashford, Kent, England) was splattered with a gold coating.

3.5. Cytotoxicity assays

3.5.1. In vitro erythrocyte lysis test

To ensure the biocompatibility of synthesized AgNPs, their cytotoxicity against RBCs was determined. The experiment initially was performed in vitro, where the AgNPs interacted with erythrocyte membranes in which membrane leakage resulted in the release of haemoglobin; disruption of the membrane led to the release of hemoglobin. Next, the amount of hemoglobin released was measured following the formula described in our previous publications (Oves et al., 2018; Ahmar Rauf et al., 2019).

3.5.2. Anticancer potential of the AgNPs

To assess the anticancer ability of Biosynthesized AgNPs, all of the cells in Leibovitz's L-15 medium, 10% FBS, 1% Streptomycin-penicillin solution were initially grown in the 95% moderately humidified environment, 5% CO2 containing 37 °C, to be edged. In addition to this, we selected breast cancer cells (MDA-MB-231). After 2–3 days of incubation, the bulk of cells hit a confluence of 90 percent, which was then transferred to cell culture plates for future tests, and trypsinized (0,03 percent EDTA 0.25 percent Trypsin).

3.5.3. The cell viability assay

For cell viability, the MTT test was performed. In the wells with 96 pools and incubate for overnight adhesion, a new cell culture containing 0.01 to 10^4 cells per well was transported. The cells were treated with a variable dose of AgNPs after overnight incubation, and further incubation lasted 24 h. The solution was then inserted 20 µl MTT (5 mg/mL) in each well and re-incubated in normal conditions for 4 h. Subsequently, the supernatant was withdrawn, and 200 µl of DMSO were inserted and incubated in each well for 10 min. An optical density value of 490 nm was then read by a microplate reading unit (Genetix580, USA). The non-treated cells were used as a control.

3.5.4. ROS generation in MDAMB-231 cells

Oxidative stress studies have shown the mechanism of cell toxicity caused by AgNPs. DCFH-DA is the cell-permeable colouring system for calculating oxidative stress in treatable nanomaterials cells. This method tested the ROS generation of MDA-MB-231 cells. The DCFH-DA method is a cell-permeable colour. The degree of fluorescence of DCFH-DA is proportionate directly to the amount of ROS produced. Briefly, a dosage of 15 and 30 µg/ml AgNPs for the new culture of MDAMB-231, 2×10^5 cells were treated, and the incubators were in optimal condition for 12 h. These cultivated cells were subsequently exposed to DCFH-DA 20 µM and incubated at 37 °C for 30 min. In addition, these treatments were obtained and cleaned under a confocal microscope with cold PBS (Zeiss). The created ROS was also assessed based on the microplate readers' fluorescence intensity (Horst et al., 2013).

3.6. Apoptotic assays

3.6.1. Hoechst blue staining

Hoechst is a DNA dye-containing compound from the brand name Bisbenzamides 33342. (BD BIO, MO, USA). After the application of AgNPs, the Hoechst stain determined the defragmentation of nuclear DNA. After 24 h of incubation, Hoechst dye (a 1:1000 dilution ratio) was processed and subsequently re-incubated under dark conditions for 10 min. The cells collected were fixed with paraformaldehyde by 4 percent, incubated at room temperature for 30 min, and washed with PBS. Confocal laser microscopy (Zeiss) was used to examine cell morphology (Yin Win and Feng, 2005).

3.6.2. Assay of mitochondrial membrane potential

Mitochondrial membrane potential was measured using Rhodamine 123. Cells were exposed to Rhodamine 123 in single-cell suspension cells from various AgNPs treated groups. A final step of the process was to have these cells washed two times with PBS, followed by analyzing the fluorescence intensity of Rhodamine-123 (Salehi et al., 2020).

4. Results

4.1. Materials characterization

4.1.1. Biogenic nanomaterials synthesis optimization and characterization

Biological assisted silver nanoparticle fabrication is a fascinating work nowadays. The aqueous solution of $AgNO_3$ and aqueous fruit extract was used initial precursor for the synthesis of material. The silver nanoparticle fabrication reaction mixture optimization at different temperatures was incubated variable period of incubation (Fig. 2). During the optimization, a good shape of the peak has appeared between 410 and 443 nm at 30 °C temperature (Fig. 2 a). The further reaction was incubated at 30 °C temperature for different periods up to 90 min. (Fig. 2 b). For the right results, a 1 ml plant extract with 100 ml of 0.1 M aqueous silver nitrate solution optimized the reaction mixture incubation for 30 min at 30 °C (Fig. 2 c). Most of the silver ion Ag + reduced to Ag0 in the nano elemental form in the solution mixture. The reaction mixture colour becomes dark brown, indicating the formation of nanomaterial inside the solution. The stability of nanomaterials was also tested after the 50 Days of fabrication.

4.1.2. Ftir and X-ray diffraction analysis

The biogenic silver nanomaterials have been synthesized from the biological moieties for the FTIR measurements to identify the *Conocarpus Lancifolius* fruits extract's possible biomolecules' and their possible involvement. FTIR spectra of dried AgNPs are shown in Fig. 3**a**. The variation in the spectrum pattern of FTIR confirmed the involvement of plant extract in the fabrication of silver nanomaterial. The spectrum pattern from the fruits extract was observed at 620, 1070, 1250, 1485, 1490, 1560, 1620, 1735, 1860, 2360, 2800, 2950, 3570 3650 and 3810 cm^{-1}, respectively. The peaks are moved to the higher wavenumber side after the biogenic manufacture of nanomaterials, such as 650, 1080, 1270, 1490, 1520, 1590, 1650, 1765, 1880, 2370, 2820, 2980, 3590 3680, and 3850 cm^{-1}. The peak is moved to a higher wavenumber side at 650 cm^{-1} at 620 cm^{-1} of the extract, which correlates to C-Cl stretching in the alkyl group. The broad bands occur between 1050 t0 1080 cm^{-1} due to ether interactions and signify the existence of flavanones adsorbed on metal nanoparticles' surface. The strong, powerful peaks at 1350 to 1485 cm^{-1} correspond to the vibrations of the C-N stretch and the protein amide I bands in the leaf extract. The phenolic groups involved in ion replacement reaction are placed in the 1250–1270 and 1485–1620 cm^{-1} areas for the plant extract. At 1560–1590 cm^{-1}, the huge band is C = C stretching in the aromatic ring, confirming the aromatic group's existence. The O-H silver nanoparticles in the vibration of carboxylic acids are moved from 3680 to 3850 cm^{-1}.

The XRD patterns of dried AgNPs have been analyzed, and the crystalline form of biogenic silver nanomaterials has been observed. The XRD indicates the number of peaks at $2 \times 30°$, 36°, 46°, 65° and 78° angles that could lead to the reflections of the 110, 111, 211, 222, and 311 lattice planes, which approximately matched the spherical shape of the silver nanomaterial crystalline structure (Fig. 3**a**). The other unsigned peak spectrum series was related to organic species' existence from the *Conocarpus Lanci-*

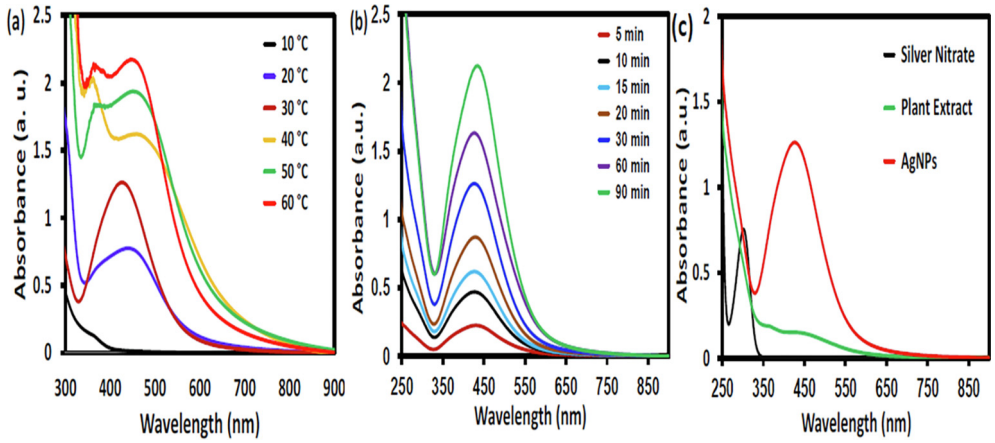

Fig. 2. Biogenic silver nanoparticles preparation optimization at (a) different temperatures, (b) variable time function, and (c) an optimized plot of silver nanoparticles formation peak.

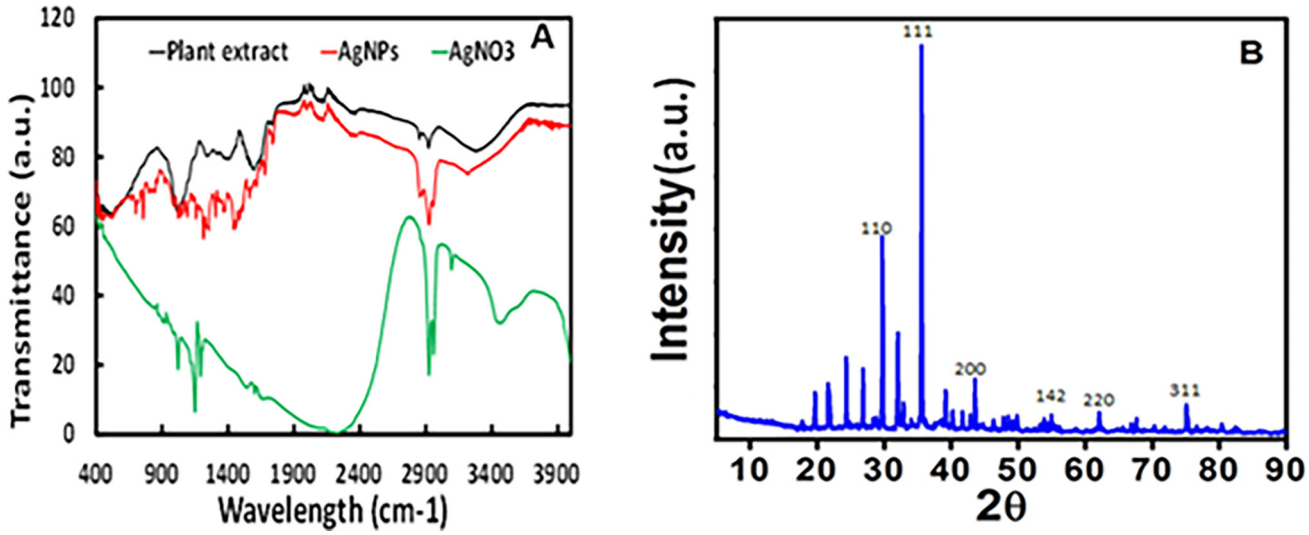

Fig. 3. Characterization of biogenic silver nanoparticles by standard techniques (A) FTIR analysis of the as-synthesized silver nanoparticles from plant extract. (B) The crystallinity of synthesized silver nanoparticles by X-ray diffraction analysis; the peak observed at 2Ø degrees with 110°, 111°, 211°, 222°, and 311°.

folius fruit extract. The analyzed data showed that the crystalline particle size was 22.5 nm in the mean diameter. The products' specific phase width is generally directly proportional to the average size of the crystalline substance. Broader peaks indicate the role of fruit extract in crystal nucleus growth and particle forming in our findings.

4.1.3. Morphological and elemental analysis of AgNPs

Electron microscopy was employed to detect the morphology of biogenic silver nanomaterials. The scanning electron microscopy (SEM) coupled with the dispersive energy X-ray (EDAX) was used to observe the material morphology and elemental constituent material at a particular point. The SEM analysis obtained image at 1 μm scale and 10000 × magnification show that a very massive amount of particle aggregates parallel EDX was used to detect the weight wise 2.09 % silver role in nanomaterials remain other elements (Fig. 4 **a & b**). In this study, the particle size between 5 and 30 nm and spherical shape was analyzed by transmission electron microscopy (TEM) depicted in Fig. 4**c**. The essential information at a particular point in the electron microscopy during sample analysis showed the nonmetallic residues confirmed biological moieties' involvement from the plant extract during the particle formation (Fig. 4**d**).

NANOPHOX particle size analysis was used to determine the particle size distribution in an aqueous suspension (Symantec GmbH). Photon cross-correlation spectroscopy is a relatively modern technique for calculating particle size, stability, and distribution in an opaque solution. It was introduced here because it is recommended for heavily diluted samples and allows accurate separation of single and multiply scattered fractions based on special scattering geometry and the scattered light's cross-correlation. Photon Cross-Correlation Spectroscopy (PCCS) NANOPHOX was used to analyze particle size and their distributions in the reaction mixture (Sympatico GmbH, Germany). In colloidal suspension, mean particle diameter (1.90258 × 50 = 26.28), particle size distribution (q3Ig = 5.29), Sauter mean diameter (SMD = 29.04 nm), mean volume diameter (VMD = 44.69), real surface area (Sv = 206.59 m^2/cm^3) and particle density were found (Fig. 6) and summarized in Table 1 for information.

4.2. Antimicrobial activity

4.2.1. Zone inhibition study

In this study, biologically synthesized silver nanomaterials were analyzed as antimicrobial agents against bacteria and fungi. For the antimicrobial testing, *Streptococcus pneumonia* and *Staphylococcus*

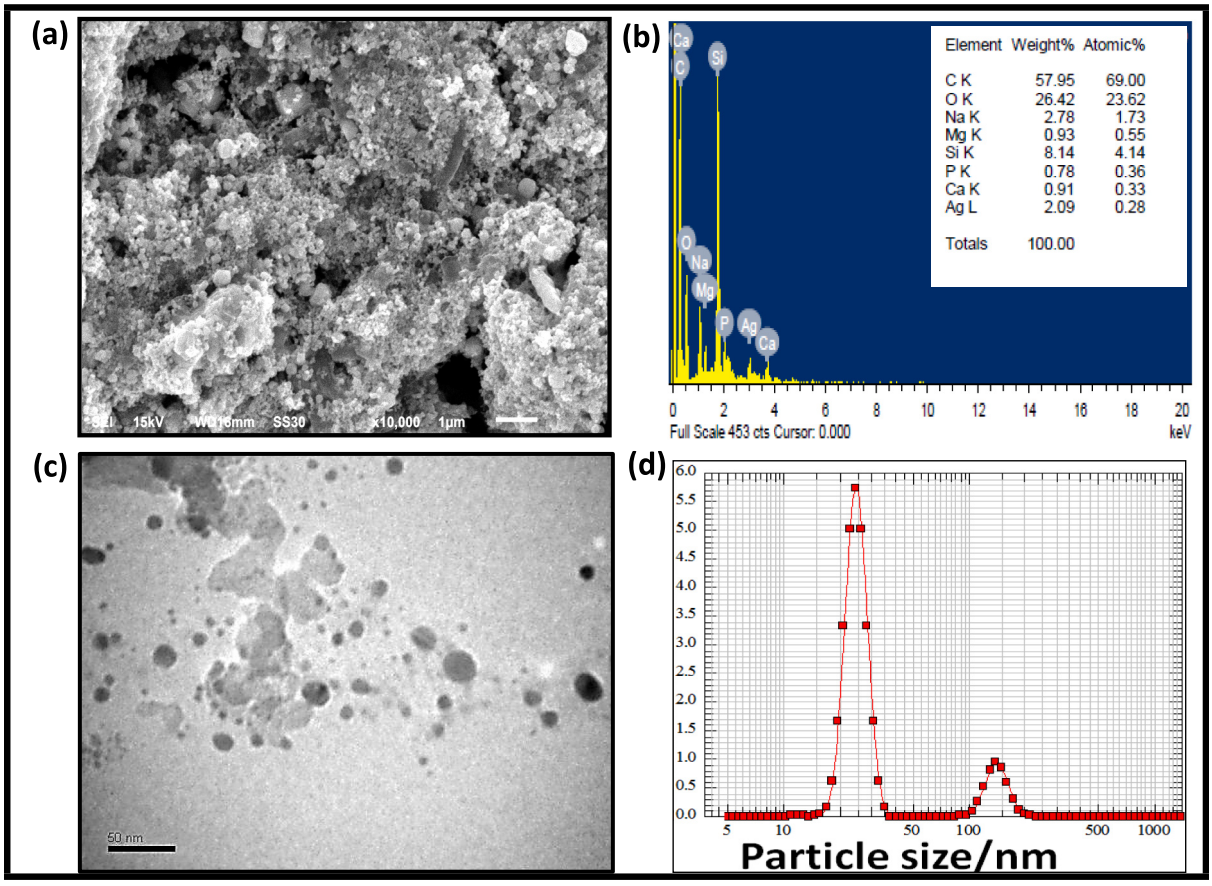

Fig. 4. Biogenic AgNPs (a) electron microscopic image scanning (b) energy dispersive X-ray demonstrating silver presence in synthesis (c) electron microscopic image at a scale of 50 nm and (iv) peak distribution of particle size often showing particle size between 21 and 173 nm. All the experiments were performed in triplicate.

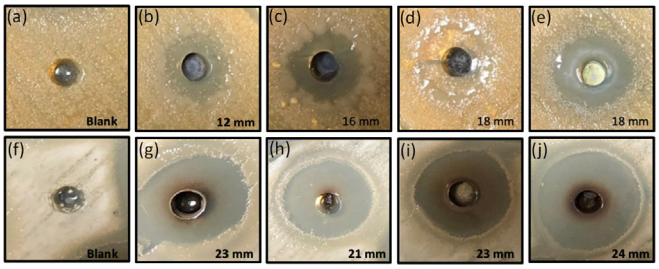

Fig. 5. Agar diffusion assay: The antimicrobial activity of biogenic AgNPs against Streptococcus pneumonia and Staphylococcus aureus bacterial strain is showed in the form of zone inhibition on a solid nutrient agar plate. The highest zone of inhibition against Streptococcus pneumonia and Staphylococcus aureus were 18 and 24 mm, respectively. The agar plate A represents the Streptococcus pneumonia untreated, whereas; the plate F represents untreated Staphylococcus aureus. Panel B to E represents the bacterial strain Streptococcus pneumonia being treated with AgNPs at a concentration of 50 μg/ml. In contrast, Panel G to J represents Staphylococcus aureus at 50 μg/ml. The zone of inhibition assay has been performed in a quadruplicate to achieve the best standard results. All the experiments were performed in triplicate and represented as ± SEM.

aureus bacterial strains were employed. In the presence of biogenic silver nanomaterial, bacterial growth becomes inhibited on the same surface as a solid nutrient agar plate (Fig. 5). Both bacterial strains, *Streptococcus pneumonia* and *Staphylococcus aureus,* showed excellent zone inhibition against the nanomaterials, increasing concentration in the well on the media plate's surface. Initially, wells showing no zone inhibition around the well in figure (Fig. 5 **a & e**) as a negative control without nanomaterials and the highest zone inhibition 18 mm against the *Streptococcus pneumonia* (Fig. 5**d**) and 24 mm against the *Staphylococcus aureus* (Fig. 5**h**) when treated with a concentration of 50 μg/ml. The creation of zone inhibition around the well due to the diffusion of nanomaterials around the well and preventing bacterial growth is depicted in a blank form zone without bacterial growth. Previously, the zone of inhibition was performed at an increasing dosage, and the concentration of 50 μg/ml was standardized [data not shown].

4.3. Fungal colony growth inhibition

AgNPs were strongly inhibited by the *Rhizopusus stolonifera* colony *and Aspergillus flavus*, as seen in Fig. 6. The colony number and size, along with a growing concentration of AgNPs, steadily decreased. At 100 μg/mL, the diameter descended to its lowest value (4 mm). The calculated IC50 of AgNPs was up to 60 μg/mL. Inhibition rate due to the varying concentrations of AgNPs (25–100 μg/mL) of *Rhizopus stolonifera* and *Aspergillus flavus* colonies. The inhibition effect is never the same; many parameters, including AgNP species, AgNP form, AgNP scale, AgNP concentration, and pathogen species, can be affected.

4.4. Biogenic silver nanomaterials with bacterial interfacial interaction study

The effect on cell morphology was investigated further to better understand the antimicrobial activity and microorganism association with nanomaterials. For this study, the bacterial strains treated with nanomaterial at fixed concentrations (50 μg /mL AgNPs).The effect of the concentration of AgNPs on cell viability

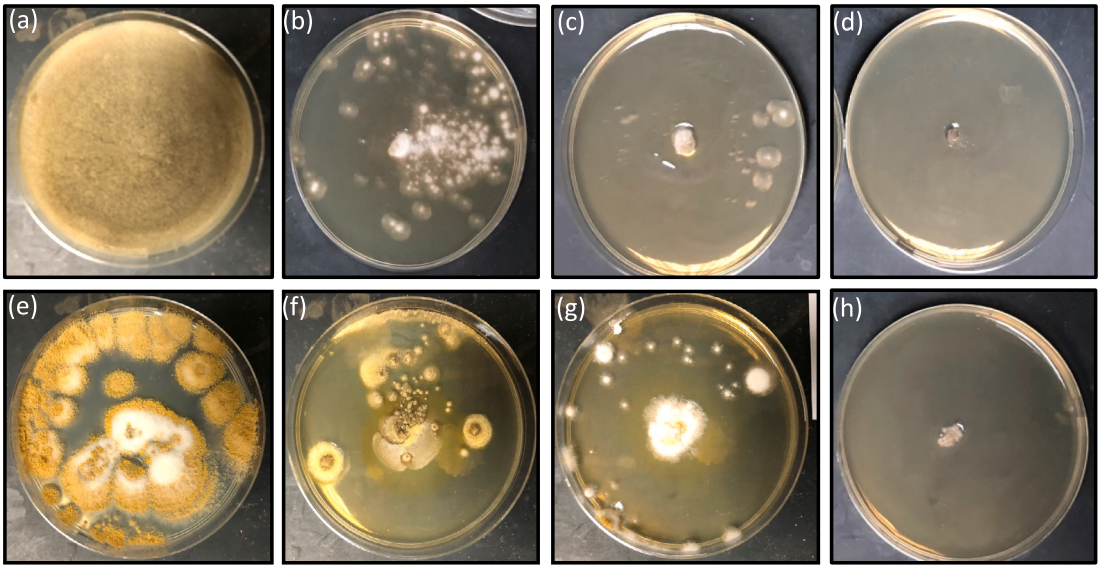

Fig. 6. The depiction of biogenic silver nanomaterials' antifungal effect at different concentrations (0,25,50 and 100 μg/ml media in plate) against *Rhizopusus stolonifera* (a to d) and *Aspergillus flavus* (e to h). All the experiments were performed in triplicate.

Table 1
In this analysis, biogenic silver nanoparticle features have been achieved.

Biogenic AgNPs		Features
Source		Lancifolius fruits
Synthesis method		Bottom-up approach
Stabilizing/capping agent		Aqueous fruit extract
Preparation period		30 min
Nanoparticle size		21–173 nm
UV–Vis (λ_{max})		410–442 nm
Mean particle diameter	x_{10}	21.54 nm
	x_{50}	26.28 nm
	x_{90}	134.95 nm
Particle size distribution (q^3lg)		5.29
Sauter mean diameter (SMD)		SMD = 29.04 nm
Volume mean diameter (VMD)		VMD = 44.69 nm
Specific surface area (Sv)		S_V = 206.59 m^2/cm^3
viscosity:		0.85 mPas
Stability		90 days
Phase		Red-brown colloidal
Biocompatible		Positive
Anticancer (IC_{50})		>30 μg/ml against MDA MB-231
Antibacterial		*Streptococcus pneumonia* and *Staphylococcus aureus*
Antifungal		*Rhizopus stolonifera* and *Aspergillus flavus*

was assessed by comparing control scanning electron microscopy images and cultures treated with AgNPs. Significant growth inhibition was found in treating *Streptococcus pneumonia* and *Staphylococcus aureus* strains with 50 μg/mL AgNPs and 48 h incubators (Fig. 7**a & e**). The efficacy of AgNPs against both bacterial strains was also tested, and 100 percent microbicidal at 60 μg/ml was found. The findings shown in the diagram (Fig. 7 at different magnification) suggest the bacterial cells' clumping/aggregation (Fig. 7 **d** and **7 g**). Images of these species treated with AgNPs showed cell death with the disintegration of cell walls by rupturing membranes or blebs. These findings verified the incorporation of AgNPs into microbe membranes and the production of membrane lipid free radicals that enhance cell autolysis. Therefore, the permeability of membrane modifications allowed str*eptococcus pneumonia* and *Staphylococcus aureus* membrane degradation. In addition, culture growth activity was also in the presence of AgNPs on the nutrient agar plate by culture spread plate system and found that the increased dose of AgNPs enhances bactericidal activity with plate with diminishing colonies.

4.5. Effect of AgNPs on the MDAMB-231 cells viability and RBC lysis

The apoptotic potential of AgNPs was ascertained employing Hoechst 33,342 staining. The treated cells were examined for nuclear morphology. The control group cells had round and homogeneously stained nuclei, while cells exposed to different AgNPs showed marked DNA condensation and apoptotic bodies. **(**Fig. 8**A**). Additionally, the cytotoxicity of AgNPs as determined by the MTT assay was concentration- and time-dependent on MDA MB-231 cells. The cells showed 18% and 12% viability at a 50 μg/ml concentration when incubated with AgNPs for 24 and 48 h, respectively **(**Fig. 8**B).** The reduction of MTT decreases with an increase in the concentration of AgNPs. The IC50 value at 24hr was 16.8 μg/ml. RBC lysis was then performed on human erythrocytes to investigate the biocompatibility of the synthesized AgNPs. It was observed that biologically synthesized AgNPs did not show high cytotoxic effects on Blood cells even at the dose of ~ 50 μg/ml (Fig. 8**C**). However, exposure of cells to increasing amounts of AgNPs resulted in decreased cell viability. Thus, the obtained

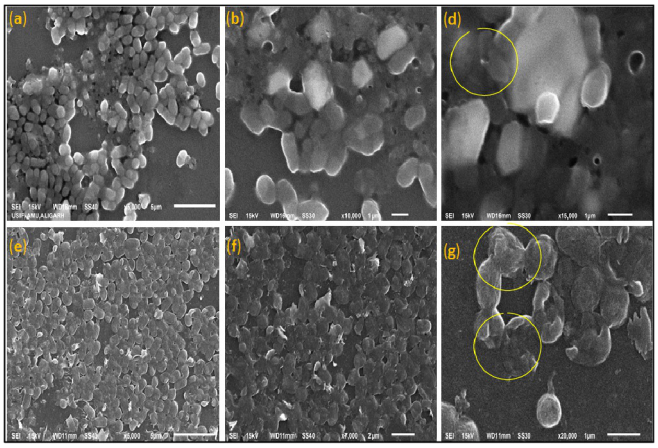

Fig. 7. The depiction of 50 μg/ml silver nanomaterials effect on the bacteria *streptococcus pneumonia* from (a) to (d) and *staphylococcus aureus* from (e) to (g) at different magnification at 5000 × to 20000 × revealed by Scanning electron microscopy. All the experiments were performed in triplicate.

results suggested the appropriateness of biologically synthesized AgNPs as a stable and nontoxic entity.

4.6. AgNPs induce ROS production in treated cells

ROS production is considered the primary mechanism for metallic nanoparticle activities that cause alteration and defragmentation of cellular proteins, DNA, and lipids that result in cell death. Therefore, to evaluate the ROS production by AgNPs (such as hydrogen peroxide and superoxide anion), a DCFH-DA dye method has been used. DCFH-DA is oxidized and changed into a highly fluorescent derivative, easily detected with a fluorescence microscope. As shown in Fig. 9, a significant increase in DCFH-DA fluorescence was observed in MDA MB-231 cells after 12 hr exposure to AgNPs compared to untreated cells understudied concentrations. Compared to untreated MDA-MB-231 cells, treated cells showed higher expression. It proves that AgNPs are responsible for ROS production that is a plausible mechanism for their anticancer activity.

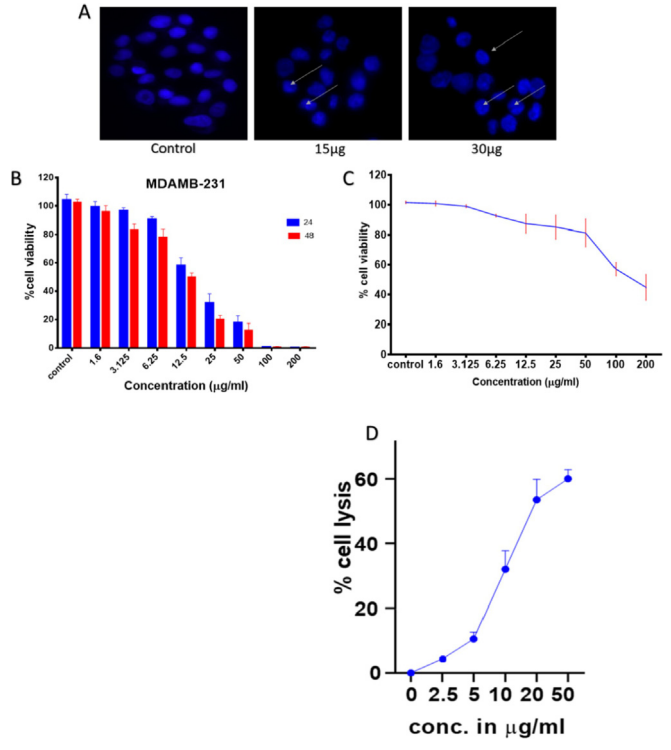

Fig. 8. Effect of Ag NPs cancer cells viability (a) Cells was treated with varying concentrations of AgNPs (15 and 30 μg/ml) for 24 hrs. DNA damage was observed by the marked punctuated fluorescence as observed in Fluorescence microscopy for Hoechst staining. (B) **MTT Assay analysis:** Cancer cells were exposed to different concentrations of AgNPs for 24 and 48hr. The data are expressed as mean § SD of three independent experiments. (C) Effect of AgNPs on the RBC lysis activity. (D) Effect of chemically synthesized AgNPs on the RBC lysis activity. All the experiments were performed in triplicate and data are described as mean § SD of three independent experiments.

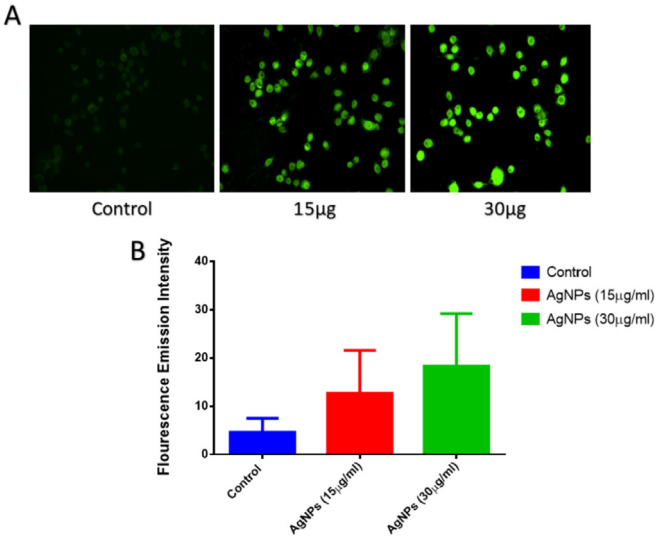

Fig. 9. The effect of Ag NPs on the cellular ROS generation (i) Cells were treated with varying concentrations of AgNPs (15 and 30 μg/ml) for 24 hrs. The Fluorescence of DCF measured ROS levels as observed in Fluorescence microscopy. Data are reported as a fold increase in DCF Fluorescence to controls. All the experiments were performed in triplicate and data are expressed as mean § SD of three independent experiments.

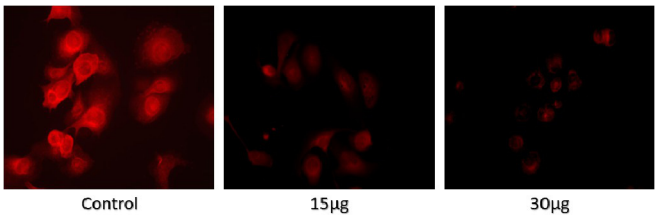

Fig. 10. Effect of AgNPs on the mitochondrial potential of the cancer cells. Cells were treated with varying concentrations of AgNPs (15 and 30 μg/ml) for 24 hrs. A decrease in the fluorescence of the rhodamine dye represents cell apoptosis. All the experiments were performed in triplicate.

4.7. Mitochondrial membrane potential reduction in AgNPs treated cells

Mitochondrial dysfunction has been associated with the activation of apoptosis. MDA-MB-231 cells from various treated groups were observed to express MMP activity. The uptake of Rhodamine 123 was measured in cancer cells using fluorescence microscopy. Reduction in colour intensity represents a decrease in MMP and is a precursor to cell death, apoptosis. Groups treated with AgNPs showed lower levels of MMP activity as compared to controls. Cells treated with 30 mg/ml of AgNPs exhibited the most significant

reduction in red fluorescence brightness compared to the other groups (Fig. 10).

5. Discussion

5.1. Plant extract and nanomaterial fabrication and its characterization

A rapid synthetic protocol was developed to synthesize highly stable AgNPs by exploiting the phytochemical reduction and stabilization capabilities in the *Conocarpus lancifolius* fruit extract. Numerous polyfunctional molecules were identified in the extract during phytochemical screening studies, including carbohydrates, proteins, amino acids, flavonoids, phenolic compounds, alkaloids, glycosides, and sugar. In the previous studies, alkaloids and aqueous extract from leaves of *Conocarpus lancifolius* were employed for the antimicrobial activities (Othman et al., 2019; Raheema and Shoker, 2020; Saadullah et al., 2020; Khan et al., 2015) but still, *Conocarpus lancifolius* fruit extract-related study not exist in the present literature. AgNPs are biocompatible due to the capping behavior of the phytochemical molecules, as revealed by cytotoxicity experiments. The trend indicates that common phytochemical constituents of the extract have been implicated in the synthesis of AgNPs. Downstream processing of the green synthesized AgNPS employing *Conocarpus lancifolius* can significantly alter the FTIR and EDAX results compared to chemically synthesized AgNPs.

Along with the lack of mechanism studies, green synthesis suffers from a shortage of cytotoxicity studies in most reports. Initially, the method was developed to produce more biocompatible AgNPs than those synthesized chemically and avoid cytotoxicity tests. The development of AgNPs was demonstrated within a short time by the apparent colour shift of the solution from colourless to dark red-brown. The rapid reduction of silver ions and stabilization of AgNPs are known to be responsible for these biomolecules. An additional change to the green chemistry approach was water as the solvent for extraction and reaction. UV–vis spectroscopy has been used to monitor the progress of the development of AgNPs. In the visible, no absorption peaks are seen for plant extract solution, and absorption peaks have been observed for AgNO3 and fabricated AgNP in solution respectively at 280 nm and 432 nm (black and red respectively in Fig. 2**).** Most of the UV–vis spectra observed were sharp and contained a single limit of SPR absorption, suggesting a small size distribution of the spherical AgNPs. Since the particles are better stabilized, there is no aggregation, so UV–vis spectral analysis corroborates the special capping effect of the phytochemicals present in the fruit extract. More details related to synthesized material summarizes in Table 1. In the previous study, silver nanomaterials have also synthesized from the mango inflorescences and date plant root (Oves et al., 2018; Qayyum et al., 2017).

After reaction with AgNO3 and fruit extract are shown in image spectral analysis, reveals a slight shift in the spectra's peak direction (Fig. 3**a**). The peaks 620, 1070, 1250, 1485, 1490, 1560, 1620, 1735, 1860, 2360, 2800, 2950, 3570 3650 and 3810 cm^{-1}, respectively, were detected in the spectrum pattern from the fruit extract. The peaks are moved to the higher wavenumber side after biogenic nanomaterial manufacture, such as at 650, 1080, 1270, 1490, 1520, 1590, 1650, 1765, 1880, 2370, 2820, 2980, 3590 3680, and 3850 cm^{-1}. Our FTIR spectral analysis findings are consistent with Basu et al. (2016) and Shankar et al. (2004), who identified similar trends in the synthesized AgNPs FTIR spectra from the green material extract. This suggests Ag's binding and capping from the plant extract with biological functional groups such as N H and OH groups. These results are in line with other experiments in which the spectral peak was found between 2820 and 3590 cm-1 and subsequent vibrations of 1° and 2° amines, amides, alcohol, and H-bonded phenols corresponding to N H and O H (Ankamwar et al., 2005). At 1270 to 1650 cm^{-1}, the absorption peak of AgNPs spectra shows C H stretching alkene vibrations (Pacioni et al., 2015), while at 1080–1270 cm^{-1}, the peak reflects the C H in-plane bending of alkenes, alcohols, carboxylic acids, esters, and ethers (Pacioni et al., 2015). Ankamwar et al. (Shankar et al., 2004) have also studied the role of bio-molecules in core particle matter. Spectra showed a band at 2370 cm^{-1} in their study and was assigned to the N- H stretching band in silver nanoparticles' free amino groups. In our sample, the spectral peak at 1590 cm^{-1} is prominent and suggests protein amide bond (C = O) involvement as a capping agent and stabilization of AgNPs. In addition to other peaks in the plant extract range, the peak present at 650–1080 cm^{-1} for the AgNPs spectrum shows the bonding of AgNPs with oxygen from the O-H. Groups into the fruit extract. This result was justified by reducing Ag + by the biological functional group previously stated by Wani et al. (2011) and stabilizing the nanomaterial. XRD pattern study of the synthesized AgNPs confirmed the crystalline nature of nanoparticle. At the variable wavelength, various peaks occurred at the 2 theta angle during the sample study. These reflections correlate well with the thoughts of Bragg. The XRD patterns of dried AgNPs were analyzed and observed the biogenic silver nanomaterials structure crystalline. The XRD reveals the number of peaks at 2θ values of 30°, 36°, 46°, 65°, and 78° angles might be related to the reflections from the 110, 111, 211, 222, and 311 lattice planes, which approximately matched with the spherical shape of the crystalline structure of silver nanomaterial (Fig. 3**b**). In addition, the peaks present at 20° and 30° show as an unassigned peak in the AgNPs range show the participation in the material synthesis of biological moieties of fruit extract. The analyzed data indicates the crystal size of nanomaterials observed in particle shape at 5–20 nm. Relevant phase widths of materials are usually directly proportional to the mean size of the crystalline substance. The smaller crystallite size (Swanson, 1953; Becheri et al., 2008) is representative of the more significant peaks. Broader peaks in our findings suggest date plant extract in crystal nuclei and particle formation growth. This outcome is also well in line with the XRD trends found by Oves et al. (2017).

The SEM and TEM analyzed the surface morphology of the biogenic nanomaterials (Fig. 4). The vacuum oven-dried materials were mounted on the SEM grid. They studied material at 15 Kv and 10,000 × magnification (and Elemental analysis done by the coupled energy-dispersive X-ray-diffraction (EDX) (Fig. 4 **a and b**). The elemental analysis reveals the highest percentage of 57.95, 26.42, and 2.09 of C, O, and Ag. The highest rates of carbon and oxygen disclose the material synthesized from the biological route. Additionally, the TEM was used to analyze biogenic nanomaterials and observed the spherical shape of a nanomaterial at a 50 nm scale (Fig. 4**c**). The size of the synthesized AgNPs identified by us is consistent with Bar et al. (2009) and Oves et al. (2020), who also reported 50 nm of AgNPs from the date root and Jatropha *curcas* plant extract (Oves et al., 2020). In addition, aqueous suspension particle size distribution was studied by NANOPHOX particle size analysis (Sympatec GmbH). Photon cross-correlation spectroscopy is a relatively modern technique for calculating particle size, stability, and distribution in opaque solutions (Fig. 4**d**). The particles details particle size distribution (q^3Ig = 5.29), Mean particle diameter ($\times_{50}$ = 26.28), Sauter mean diameter (SMD = 29.04 n m), specific surface area (Sv = 206.59 m^2/cm^3), volume mean diameter (VMD = 44.69), and particle density was found in colloidal suspension. The data validate with the previously published article nanoparticles synthesized from the bacterial extract (Oves et al., 2018).

5.2. Antimicrobial studies

To investigate the effect of the green synthesized nanomaterial on microbial growth inhibition, the synthesized AgNPs were tested against bacterial and fungal strains. Applied nanomaterials concentration developed a zone of inhibition around the wells' loaded material (Fig. 5). Both bacterial strains, *Streptococcus pneumonia* and *Staphylococcus aureus*, showed excellent zone inhibition against the nanomaterials, increasing concentration in the well on the media plate's surface. Initially, wells showing no zone inhibition around the well in figure (Fig. 5 **a & e**) as a negative control without nanomaterials and the highest zone inhibition 18 mm against the *Streptococcus pneumonia* (Fig. 5**d**) and 24 mm against the *Staphylococcus aureus* (Fig. 5**h**). The inhibition zone observed in *Staphylococcus aureus* was significant than reported by Maziya et al. (2020) & Maity et al. (2020) and compared to AgNPs synthesized through chemical method **[SI 1].** *Streptococcus pneumonia* results are under Amro et al. (2000), who has rapid biosynthesis of silver nanoparticles from the green stem of *Andrographis paniculata* (Kalmegh) and their antibacterial activity on multi-drug resistant clinical pathogens? Our findings are consistent with Banu et al. (2011); they clarified that the depletion of metals from microbial cells might contribute to pores or creases on the outer surface. Such pits are formed by repeatedly releasing molecules of lipopolysaccharides and membrane proteins. Therefore, the permeability of the membrane modifications can induce bacterial membrane fragmentation (Qayyum et al., 2017).

AgNPs were strongly inhibited by the *Rhizopusus stolonifera* colony *and Aspergillus flavus*, as seen in Fig. 6. The previously amended silver nanomaterial prevents the growth of the fungal colony. The colony number and size, along with a growing concentration of AgNPs, steadily decreased. At 100 μg/mL, the diameter descended to its lowest value (4 mm). The calculated IC50 of AgNPs was up to 60. Of μg/ml. Inhibition rate due to the varying concentrations of AgNPs (25–100 μg/mL) of *Rhizopus stolonifera* and *Aspergillus flavus* colonies. The antifungal activity of our synthesized AgNPs is also significantly collinear with earlier reports (Abdelghany et al., 2020; Gurunathan et al., 2013).

5.3. Anticancer activities

5.3.1 AgNPs induce ROS production in treated cells

The apoptotic potential of the AgNPs was determined by Hoechst-33342 staining. The nuclear morphology of the treated cells was examined. The control group cells had round and homogeneous nuclei, while cells exposed to different AgNPs showed clear DNA condensation and apoptotic bodies. Additionally, the MTT test demonstrated that AgNPs cytotoxicity on MDA MB-231 cells was concentration- and time-dependent (Abdal Dayem et al., 2017). The cells showed 18% and 12% viability at a 50 μg / ml concentration when incubated with AgNPs for 24 and 48 h, respectively. The reduction of MTT decreases with the increasing concentration of AgNPs. The IC50 value at 24hr was 16.8 μg/ml. Following that, human erythrocytes were lysed to determine the biocompatibility of synthesized AgNPs. It was observed that biologically synthesized AgNPs did not exhibit high cytotoxic effects on blood cells even at a dose of approx. 50 μg / ml compared to the chemically synthesized AgNPs [Fig. 8] However, the exposure of cells to increasing doses of AgNPs resulted in reduced cell viability. Thus, the obtained results suggested the appropriateness of biologically synthesized AgNPs as a stable and nontoxic entity [Fig. 8].

ROS generation is considered the critical mechanism for metallic nanoparticles' activities that cause cellular proteins, DNA, and lipids peroxidation, resulting in cell death (Azizi et al., 2017). ROS are chemically reactive particles that contain oxygen, including hydrogen peroxide (H2O2), reactive superoxide anion radicals ($\mathbf{O_2^{\cdot}}$), and hydroxyl radicals (·OH). Nevertheless, the exposure to NPs, the intracellular generation of ROS may sharply increase by inducing ROS bursts in cells. The main mechanistic explanations for ROS bursts are that metal ions released by NPs promote ROS overexpression by impairing mitochondrial respiration(Ahmar Rauf et al., 2019; Azizi et al., 2017; Botcha and Prattipati, 2020). Therefore, an experimental setup based on DCFH-DA dye has been used to test the ROS production by AgNPs (such as hydrogen peroxide and superoxide anion). DCFH-DA is oxidized and converted into a strongly fluorescent derivative, readily visible under a fluorescence microscope. As seen in Fig. 9, a substantial increase in DCFH-DA fluorescence relative to untreated cells at variable concentrations was observed in MDA MB-231 cells after 12 h of exposure to AgNPs. The treated cells displayed greater expression compared with untreated MDA-MB-231 cells. The obtained results indicate that AgNPs are responsible for ROS production, which is a possible mechanism for their action against cancer. The present investigation followed a similar trend obtained by Botcha and Prattipati (2020). They observed dose-dependent cytotoxicity against MDA-MB-231 cells through activation of reactive oxygen species (ROS) generation.

The metal ions released by NPs have been shown to mix into redox cycling and chemocatalysis via the Fenton reaction [$H_2O_2 + Fe^{2+} \rightarrow Fe^{3+} + HO^- + \cdot OH$] or Fenton-like reaction [$Ag^+ H_2O_2 + H^+ = Ag^+ + \cdot OH + H_2O$]. The dissociated Ag^+ also causes cellular enzyme deactivation, membrane structure disruption disturbed electron-shuttling process, depleted redox potential levels, reduced mitochondrial membrane potentials (MMP). The activation of the apoptosis process has been linked with mitochondrial dysfunction. To express MMP function, MDA-MB-231 cells from different AgNPs treated groups were observed. Using fluorescence microscopy, Rhodamine 123 uptake was evaluated in cancer cells. A drop in MMP, a precursor to cell death, apoptosis, is marked as a decline in the Fluorescence strength. As compared to controls, AgNPs treated groups displayed lower levels of MMP activity. Compared to the other classes, cells treated with 30 μg/ml of AgNPs showed the highest decrease in the red fluorescence brightness [Fig. 10]. The obtained results also corroborated with the results observed by Botcha et al., where they synthesized plant extract mediated silver nanoparticles to perform the cytotoxicity evaluation against MDA-MB-231 Botcha and Prattipati (2020).

6. Conclusion

An aqueous fruit extract of Conocarpus Lancifolius was used to prepare mono-dispersed AgNPs in the current research. UV–visible, XRD, TEM, and FT-IR spectra have characterized the AgNPs. They have a spherical shape with an average of 26.28 nm in size. *Conocarpus lancifolius* biological synthesis of AgNPs is a cheap, non-polluting, and safe technique and is an excellent alternative to chemical and physical methods. Our findings confirmed that Conocarpus Lancifolius fruit aqueous extract might be an effective method for AgNPs' biosynthesis and stabilization of silver ions. Ag-phase at the nanoscale of spherically shaped particles. Thus, this green approach demonstrates reproducible performance, eco-friendliness, reduced reaction time, cost-effectiveness, and simplicity in producing highly stable nanoparticles with enhanced antibacterial activity—the characterized particles inhibited bacterial growth and biofilm formation at sub-MIC concentrations. SEM showed that AgNPs act on the bacterial surface and inhibit its growth. This association produces some unique ROS species, leading to bacterial cell death and growth obliteration. The overall findings reveal that biologically synthesized AgNPs have antiproliferative efficacy in the MDA-MB-231 breast cancer cell line by

inducing apoptosis, indicating that biologically synthesized AgNPs could be a possible alternative agent for treating human breast cancer.

Declaration of Competing Interest

The authors declare that they have no known competing financial interests or personal relationships that could have appeared to influence the work reported in this paper.

Acknowledgement

The authors are thankful to the Deanship of Scientific Research, King Khalid University, Abha, Saudi Arabia, for financially supporting this work through the Research Group Project under grant number (RGP.1/48/42).

Appendix A. Supplementary material

Supplementary data to this article can be found online at https://doi.org/10.1016/j.sjbs.2021.09.007.

References

"Genus: Conocarpus L." Germplasm Resources Information Network. United States Department of Agriculture. 1996-09-17. Archived from the originalon 2010-05-30. Retrieved 2010-11-27.

Abdal Dayem, A., Hossain, M.K., Lee, S.B., Kim, K., Saha, S.K., Yang, G.M., Choi, H.Y., Cho, S.G., 2017. The role of reactive oxygen species (ROS) in the biological activities of metallic nanoparticles. Int. J. Mol. Sci. 18 (1), 120.

Abdelghany, T.M., Hassan, Maryam M., El-Naggar, Medhat A., El-Mongy, Mahmoud Abd, 2020. GC/MS analysis of Juniperus procera extract and its activity with silver nanoparticles against Aspergillus flavus growth and aflatoxins production. Biotechnol. Rep, 27, e00496. https://doi.org/10.1016/j.btre.2020.e00496.

Ahmar Rauf, Mohd., Oves, Mohammad, Ur Rehman, Fawad, Rauf Khan, Abdur, Husain, Nazim, 2019. Bougainvillea flower extract mediated zinc oxide's nanomaterials for antimicrobial and anticancer activity. Biomed. Pharmacother. 116, 108983. https://doi.org/10.1016/j.biopha.2019.108983.

Ali, H.M., Salem, M.Z., Abdel-Megeed, A., 2013. In-vitro antibacterial activities of alkaloids extract from leaves of Conocarpus lancifolius Engl. J. Pure Appl. Microbiol 7 (3), 1903–1907.

Al-Taweel, A.M., Perveen, S., Fawzy, G.A., Mehmood, R., Khan, A., Khan, S.I., 2016. New ellagic acid derivative from the fruits of heat-tolerant plant Conocarpus lancifolius Engl, and their anti-inflammatory, cytotoxic. PPAR agonistic activities, Pakistan journal of pharmaceutical sciences, p. 29.

Amro, N.A., Kotra, L.P., Wadu-Mesthrige, K., Bulychev, A., Mobashery, S., Liu, G.Y., 2000. High-resolution atomic force microscopy studies of the Escherichia coli outer membrane: structural basis for permeability. Langmuir 16 (6), 2789–2796.

Ankamwar, Balaprasad, Chaudhary, Minakshi, Sastry, Murali, 2005. Gold nanotriangles biologically synthesized using tamarind leaf extract and potential application in vapor sensing. Synth. React. Inorg., Met.-Org., Nano-Met. Chem. 35 (1), 19–26.

Azizi, M., Ghourchian, H., Yazdian, F., Bagherifam, S., Bekhradnia, S., Nyström, B., 2017. Anti-cancerous effect of albumin coated silver nanoparticles on MDA-MB 231 human breast cancer cell line. Sci. Rep. 7 (1), 1–18.

Banu, Afreen, Rathod, Vandana, Ranganath, E., 2011. Silver nanoparticle production by Rhizopus stolonifer and its antibacterial activity against extended spectrum β-lactamase producing (ESBL) strains of Enterobacteriaceae. Mater. Res. Bull. 46 (9), 1417–1423.

Bar, Harekrishna, Bhui, Dipak Kr., Sahoo, Gobinda P., Sarkar, Priyanka, Pyne, Santanu, Misra, Ajay, 2009. Green synthesis of silver nanoparticles using seed extract of Jatropha curcas. Colloids Surf., A 348 (1-3), 212–216.

Barakat, M.A., Anjum, M., Kumar, R., Alafif, Z.O., Oves, M., Ansari, M.O., 2020. Design of ternary Ni (OH) 2/graphene oxide/TiO2 nanocomposite for enhanced photocatalytic degradation of organic, microbial contaminants, and aerobic digestion of dairy wastewater. J. Cleaner Prod. 258, 120588. https://doi.org/10.1016/j.jclepro.2020.120588.

Basu, Shibani, Maji, Priyankar, Ganguly, Jhuma, 2016. Rapid green synthesis of silver nanoparticles by aqueous extract of seeds of Nyctanthes arbor-tristis. Applied Nanoscience 6 (1), 1–5.

Becheri, Alessio, Dürr, Maximilian, Lo Nostro, Pierandrea, Baglioni, Piero, 2008. Synthesis and characterization of zinc oxide nanoparticles: application to textiles as UV-absorbers. J. Nanopart. Res. 10 (4), 679–689.

Bindhu, M.R., Umadevi, M., Esmail, G.A., Al-Dhabi, N.A., Arasu, M.V., 2020. Green synthesis and characterization of silver nanoparticles from Moringa oleifera flower and assessment of antimicrobial and sensing properties. J. Photochem. Photobiol., B 205, 111836. https://doi.org/10.1016/j.jphotobiol.2020.111836.

Botcha, Satyanarayana, Prattipati, Subhashini Devi, 2020. Callus extract mediated green synthesis of silver nanoparticles, their characterization and cytotoxicity evaluation against MDA-MB-231 and PC-3 Cells. BioNanoScience 10 (1), 11–22.

Conocarpus lancifolius - Geographic range in detail". IUCN Red List. 1998. Retrieved February 24, 2019.

Duke, James A. (July 8, 1996). "Conocarpus erectus L." Retrieved February 24, 2019.

Gurunathan, S., Han, J.W., Eppakayala, V., Jeyaraj, M. and Kim, J.H., 2013. Cytotoxicity of biologically synthesized silver nanoparticles in MDA-MB-231 human breast cancer cells. BioMed research international, 2013.

Horst, Allison M., Vukanti, Raja, Priester, John H., Holden, Patricia A., 2013. An assessment of fluorescence-and absorbance-based assays to study metal-oxide nanoparticle ROS production and effects on bacterial membranes. Small 9 (9-10), 1753–1764.

Khan, Aisha Saleem, 2017. In: Medicinally Important Trees. Springer International Publishing, Cham, pp. 21–53. https://doi.org/10.1007/978-3-319-56777-8_2.

Khan, Hassan Ahmed, Ahmad, Aftab, Mehboob, Riffat, 2015. Nosocomial infections and their control strategies. Asian pacific journal of tropical biomedicine 5 (7), 509–514.

Maduraiveeran, G., Sasidharan, M., Ganesan, V., 2018. Electrochemical sensor and biosensor platforms based on advanced nanomaterials for biological and biomedical applications. Biosens. Bioelectron. 103, 113–129.

Maity, Gajendra Nath, Maity, Prasenjit, Choudhuri, Indranil, Sahoo, Ganesh Chandra, Maity, Nirmal, Ghosh, Kaushik, Bhattacharyya, Nandan, Dalai, Sudipta, Mondal, Soumitra, 2020. Green synthesis, characterization, antimicrobial and cytotoxic effect of silver nanoparticles using arabinoxylan isolated from Kalmegh. Int. J. Biol. Macromol. 162, 1025–1034.

Maziya, Khona, Dlamini, Bhekisisa C., Malinga, Soraya P., 2020. Hyperbranched polymer nanofibrous membrane grafted with silver nanoparticles for dual antifouling and antibacterial properties against Escherichia coli, Staphylococcus aureus and Pseudomonas aeruginosa. React. Funct. Polym. 148, 104494. https://doi.org/10.1016/j.reactfunctpolym.2020.104494.

Mohammed, S.A., Mousa, H.M. and Alwan, A.H., 2019, July. Determination of hemolytic Cytotoxicity and Antibacterial Activity of Conocarpus Lancifolius Aqueous leaves extract. In IOP Conference Series: Materials Science and Engineering (Vol. 571, No. 1, p. 012045). IOP Publishing.

Othman, L., Sleiman, A., Abdel-Massih, R.M., 2019. Antimicrobial activity of polyphenols and alkaloids in middle eastern plants. Front. Microbiol. 10, 911.

Oves, M., Aslam, M., Rauf, M.A., Qayyum, S., Qari, H.A., Khan, M.S., Alam, M.Z., Tabrez, S., Pugazhendhi, A., Ismail, I.M.I., 2018. Antimicrobial and anticancer activities of silver nanoparticles synthesized from the root hair extract of Phoenix dactylifera. Mater. Sci. Eng., C 89, 429–443.

Oves, M., Rauf, M., Ansari, M.O., Aslam Parwaz Khan, A., A Qari, H., Alajmi, M.F., Sau, S. and Iyer, A.K., 2020. Graphene Decorated Zinc Oxide and Curcumin to Disinfect the Methicillin-Resistant Staphylococcus aureus. Nanomaterials, 10 (5), p.1004.

Oves, Mohammad, Qari, Huda A., Felemban, Nadeen M., Khan, Mohammad Z., Rehan, Zulfiqar A., Ismail, Iqbal M.I., 2017. Marinobacter lipolyticus from Red Sea for lipase production and modulation of silver nanomaterials for anti-candidal activities. IET Nanobiotechnol. 11 (4), 403–410.

Oves, M., Rauf, M.A., Hussain, A., Qari, H.A., Khan, A.A.P., Muhammad, P., Rehman, M. T., Alajmi, M.F., Ismail, I.I., 2019. Antibacterial silver nanomaterial synthesis from Mesoflavibacter zeaxanthinifaciens and targeting biofilm formation. Front. Pharmacol. 10, 801.

Pacioni, N.L., Borsarelli, C.D., Rey, V., Veglia, A.V., 2015. In: Synthetic routes for the preparation of silver nanoparticles. Springer, Cham, pp. 13–46.

Qayyum, S., Oves, M., Khan, A.U., Mukherjee, A., 2017. Obliteration of bacterial growth and biofilm through ROS generation by facilely synthesized green silver nanoparticles. PLoS ONE 12 (8), e0181363. https://doi.org/10.1371/journal.pone.0181363.

Raheema, R.H., Shoker, R.M., 2020. Phytochemicals screening and antibacterial activity of silver nanoparticles, phenols and alkaloids extracts of conocarpus lancifolius. EurAsian Journal of BioSciences 14 (2), 4829–4835.

Renuka, R., Devi, K.R., Sivakami, M., Thilagavathi, T., Uthrakumar, R., Kaviyarasu, K., 2020. Biosynthesis of silver nanoparticles using Phyllanthus emblica fruit extract for antimicrobial application. Biocatalysis and Agricultural Biotechnology 24, 101567. https://doi.org/10.1016/j.bcab.2020.101567.

Rohaizad, A., Shahabuddin, S., Shahid, M.M., Rashid, N.M., Hir, Z.A.M., Ramly, M.M., Awang, K., Siong, C.W., Aspanut, Z., 2020. Green synthesis of silver nanoparticles from Catharanthus roseus dried bark extract deposited on graphene oxide for effective adsorption of methylene blue dye. J. Environ. Chem. Eng. 8 (4), 103955. https://doi.org/10.1016/j.jece:2020.103955.

Saadullah, Malik, Asif, Muhammad, A. Ch, Bashir, Yaseen, Hafiza S., Uzair, Muhammad, Afzal, Khurram, 2020. Isolation, Characterization and Preliminary Cytotoxic and Antifungal Evaluations of Novel Lancifoliate Isolated from Methanol Extract of Conocarpus lancifolius. Anticancer Agents in Medicinal Chemistry (Formerly Current Medicinal Chemistry-Anti-Cancer Agents) 20 (14), 1664–1672.

Salehi, Fahimeh, Behboudi, Hossein, Kavoosi, Gholamreza, Ardestani, Sussan K., 2020. Incorporation of Zataria multiflora essential oil into chitosan biopolymer nanoparticles: A nanoemulsion based delivery system to improve the in-vitro

efficacy, stability and anticancer activity of ZEO against breast cancer cells. Int. J. Biol. Macromol. 143, 382–392.
Shankar, S.Shiv, Rai, Akhilesh, Ahmad, Absar, Sastry, Murali, 2004. Rapid synthesis of Au, Ag, and bimetallic Au core–Ag shell nanoparticles using Neem (Azadirachta indica) leaf broth. J. Colloid Interface Sci. 275 (2), 496–502.
Swanson, H.E., 1953. Standard X-ray diffraction powder patterns (Vol. 1). US Department of Commerce, National Bureau of Standards.
Swilam, N., Nematallah, K.A., 2020. Polyphenols profile of pomegranate leaves and their role in green synthesis of silver nanoparticles. Sci. Rep. 10 (1), 1–11.
Wani, Irshad A., Ganguly, Aparna, Ahmed, Jahangeer, Ahmad, Tokeer, 2011. Silver nanoparticles: ultrasonic wave assisted synthesis, optical characterization and surface area studies. Mater. Lett. 65 (3), 520–522.
Yaqoob, A.A., Ahmad, H., Parveen, T., Ahmad, A., Oves, M., Ismail, I.M., Qari, H.A., Umar, K., Mohamad Ibrahim, M.N., 2020. Recent advances in metal decorated nanomaterials and their various biological applications: a review. Front. Chem. 8, 341.
Yin Win, Khin, Feng, Si-Shen, 2005. Effects of particle size and surface coating on cellular uptake of polymeric nanoparticles for oral delivery of anticancer drugs. Biomaterials 26 (15), 2713–2722.